Author(s): Chmaissem, O. & Grigoraviciute, I. & Yamauchi, H. & Karppinen, Maarit & Marezio, M.

Title: Superconductivity and oxygen ordering correlations in the homologous series of (Cu, Mo)Sr2(Ce, Y)sCu2O5+2s+[delta]

Year: 2010

Version: Final published version

Please cite the original version:

Chmaissem, O. & Grigoraviciute, I. & Yamauchi, H. & Karppinen, Maarit & Marezio, M. 2010. Superconductivity and oxygen ordering correlations in the homologous series of (Cu, Mo)Sr2(Ce, Y)sCu2O5+2s+[delta]. Physical Review B. Volume 82, Issue 10. 104507/1-9. ISSN 1550-235X (electronic). DOI: 10.1103/physrevb.82.104507.

Superconductivity and oxygen ordering correlations in the homologous series of $(Cu,Mo)Sr_2(Ce,Y)_sCu_2O_{5+2s+\delta}$

O. Chmaissem,[1,2,*] I. Grigoraviciute,[3] H. Yamauchi,[3,4] M. Karppinen,[3,4] and M. Marezio[5]
[1]*Physics Department, Northern Illinois University, DeKalb, Illinois 60115, USA*
[2]*Materials Science Division, Argonne National Laboratory, Argonne, Illinois 60439, USA*
[3]*Materials and Structures Laboratory, Tokyo Institute of Technology, Yokohama 226-8503, Japan*
[4]*Laboratory of Inorganic Chemistry, Aalto University School of Science and Technology, FI-00076 AALTO, Finland*
[5]*CRETA/CNRS, 25 Avenue des Martyrs, 38042 Grenoble Cedex 9, France*
(Received 7 June 2010; revised manuscript received 17 August 2010; published 10 September 2010)

A detailed study of the structure-property relationship is reported for the first four members of the high-T_c superconducting homologous series of $(Cu,Mo)Sr_2(Ce,Y)_sCu_2O_{5+2s+\delta}$ [(Cu,Mo)-12*s*2]. In this series, the adjacent CuO_2 planes are separated by a single Y-cation layer for $s=1$ and a fluorite-type (Ce,Y)-$[O_2$-$(Ce,Y)]_{s-1}$ layer block for $s \geq 2$. Even though this series may be considered a conventional homologous series from the chemical point of view, we emphasize that the structures are different from those of the Tl-, Hg-, Bi-, etc.,-based series by the fact that the inserted fluorite-type blocks are insulating. We show the formation of the higher *s* members via intercalation of additional Ce-O_2 layer(s) into the crystal lattices of the lower members of the series. Neutron powder-diffraction data demonstrate that the Ce/Y ratio is not constant at the different (Ce,Y) layers in the fluorite-structured block and that the innermost (Ce,Y) layer(s) are significantly Ce rich compared with the outer ones. Two independent crystallographic sites are identified for the extra oxygen atoms in the basal $(Cu_{0.75}Mo_{0.25})O_{1+\delta}$ plane with site fractional occupancies that strongly correlate with the properties of the material. A short-range ordered structure is proposed for the $(Cu_{0.75}Mo_{0.25})O_{1+\delta}$ layers that could explain both the superconducting properties of the materials and the enhanced T_c for the first member of the series.

DOI: 10.1103/PhysRevB.82.104507 PACS number(s): 74.72.−h, 61.05.fm

I. INTRODUCTION

Multilayered transition-metal oxides have, for the last two decades, been extensively investigated for their ability to host a wide variety of functional properties, such as high-T_c superconductivity ($T_c \equiv$ critical superconductivity transition temperature), thermoelectricity, oxide-ionic conductivity, and high-performance magnetoresistance, etc. From the viewpoint of materials development, "layer-engineering" has proven to be a particularly successful concept for the design of many new homologous series. Most impressively, within the field of high-T_c cuprate superconductors, the huge variety of the presently known phases can be universally categorized as members of just two basic homologous families, namely, $M_mA_2Q_{n-1}Cu_nO_{m+2+2n\pm\delta}$ [or *M*-*m*2(*n*-1)*n*] and $M_mA_2B_sCu_2O_{m+4+2s\pm\delta}$ [*M*-*m*2*s*2], where *M*=Cu, Bi, Pb, Tl, Hg, etc.; *A*=Ba, Sr, La; *Q*=Ca, rare-earth (*R*) element; and *B*=(Ce,*R*).[1] Thus, each homologous family may serve as a platform for the next-stage design of new materials that can be fabricated by the simple addition or removal of one or more atomic layers into or out of already known structures or by the partial replacement of some constituent layers by other layers with different chemical compositions.

To this date, more than 20 independent homologous series of the *M*-*m*2(*n*-1)*n* type have been established (i.e., at least three members of a series have experimentally been isolated). The *M*-*m*2(*n*-1)*n* family is by far more common than *M*-*m*2*s*2. In this family, the members of one series vary by the layer number (*n*) of consecutively stacked CuO_2 planes in the superconductive CuO_2-$(Q$-$CuO_2)_{n-1}$ block. Homologous series Bi-22(*n*-1)*n* (Refs. 2 and 3) was the first of this type but it was immediately followed by the T_c record breaking Tl-22(*n*-1)*n*, Tl-12(*n*-1)*n*, and Hg-12(*n*-1)*n* series.[4–10] Interestingly, all the presently known *M*-*m*2(*n*-1)*n* homologous series achieve a maximum T_c for $n=3$ followed by slowly decreasing T_c values when *n* exceeds 3.[1] However, one may argue that the higher *n* members of the series may not necessarily be optimized with respect to proper hole-doping levels and accordingly the comparison with the lower *n* members may not be completely meaningful. As for the formation mechanism of the *M*-*m*2(*n*-1)*n* phases, it is reasonable to anticipate that the higher *n* members form by the intercalation of additional CuO_2-*Q* layer units (i.e., nominally neutral layers where *Q* is a divalent cation) into the lower *n*-member structures.

In the *M*-*m*2*s*2 family, the members in a series differ from each other by the number (*s*) of the *B* cation, i.e., the (Ce,*R*) layers in the fluorite-structured (Ce,*R*)-$[O_2$-$(Ce,R)]_{s-1}$ block located between two adjacent CuO_2 planes.[1] Several series have been reported, e.g., (Pb,Cu)-32*s*2,[11,12] (Fe,Cu)-12*s*2,[13] Co-12*s*2,[14] Ru-12*s*2,[15–17] and (Hg,W)-12*s*2 (Refs. 18 and 19) but, to this date, most members of such series were not fully or properly characterized. The increasing thickness of the (Ce,*R*)-$[O_2$-$(Ce,R)]_{s-1}$ block, as *s* increases beyond 2, makes it progressively more difficult to obtain high-quality superconducting samples. Nonetheless, we recently succeeded in synthesizing high-quality single-phase samples for the first four members of the $(Cu_{0.75}Mo_{0.25})Sr_2(Ce,Y)_sCu_2O_{5+2s+\delta}$ series [(Cu,Mo)-12*s*2] and in inducing superconductivity in all the samples by postsynthesis high-pressure oxygen annealing.[20] In this paper, we report detailed crystal structures for the four phases

as determined by neutron powder diffraction (NPD). We discuss the phase formation mechanism and the evolution of the crystal and chemical surroundings around the CuO_2 planes and within the basal $(Cu,Mo)O_{1+\delta}$ planes upon increasing s.

II. EXPERIMENTAL DETAILS

A. Materials synthesis

Samples of the first four (Cu,Mo)-12s2 members, i.e., $(Cu_{0.75}Mo_{0.25})Sr_2YCu_2O_{7+\delta}$ ($s=1$), $(Cu_{0.75}Mo_{0.25})Sr_2(Ce_{1/2}Y_{1/2})_2Cu_2O_{9+\delta}$ ($s=2$), $(Cu_{0.75}Mo_{0.25})Sr_2(Ce_{2/3}Y_{1/3})_3Cu_2O_{11+\delta}$ ($s=3$), and $(Cu_{0.75}Mo_{0.25})Sr_2(Ce_{3/4}Y_{1/4})_4Cu_2O_{13+\delta}$ ($s=4$) were synthesized using homogeneous nitrate precursors prepared from appropriate amounts of CuO, MoO_3, $SrCO_3$, CeO_2, and Y_2O_3 powders. Detailed synthesis procedures can be found elsewhere.[20] Briefly, the starting powders were dissolved in an aqueous solution of 2M HNO_3 and 0.1M H_2O_2. Evaporation of the solvent at ~100 °C resulted in a black solid nitrate residue which was then decomposed and calcined through subsequent short-time annealing periods at 220, 450, 650, 850, and 900 °C with intermediate grindings. The final firing was performed in air in several steps, for $s=1$ at 930–960 °C (for a total of 72 h), for $s=2$ at 950–1005 °C (120 h), for $s=3$ at 950–1005 °C (168 h), and for $s=4$ at 950–985 °C (264 h).

B. High-pressure oxygenation

In order to render them superconducting, the as-synthesized (AS) samples were high-pressure oxygenated (HPO) in a cubic-anvil-type high-pressure cell at 5 GPa and 500 °C for 30 min in the presence of 33 mol % $KClO_3$. Under high pressure, $KClO_3$ decomposes to KCl and oxygen and acts as an efficient extra-oxygen source. Prior to arriving at this "critical" value, many high-pressure experiments were performed in which we observe that T_c gradually increases to 87 K (for $s=1$) or to 54–56 K (for $s=2-4$) as we gradually increase the amount of $KClO_3$ to 33 mol %. For larger amounts of $KClO_3$ all four members of the series started to decompose. Thus, we conclude that our HPO samples have either reached their optimal-doping level or were on the verge to becoming optimally doped but not overdoped. More experiments may be needed to fine tune and pinpoint the exact amount of $KClO_3$ needed to optimally dope every member of the series. Characterization of the HPO samples proved the uniformity and high reproducibility of the HPO treatment.

Superconducting samples ($s=1-3$) were prepared for neutron powder-diffraction experiments by combining several high-pressure oxygenated specimens (~70 mg each) taken from the same AS sample. Unfortunately, the lengthy synthesis procedures of a sufficiently large sample suitable for NPD of the superconducting $s=4$ phase did not allow us to determine the detailed structure of the HPO $s=4$ member. Nevertheless, it was characterized by x-ray powder diffraction (XRD) and magnetic-susceptibility measurements.

C. Characterization of intermediate products

In order to monitor the phase formation process during synthesis, XRD data were collected at intermediate synthesis steps using a Rigaku RINT2550VK/U diffractometer equipped with a rotating Cu anode. The superconducting properties of the samples were measured for both the intermediate and the final single-phase products using a superconducting-quantum-interference device magnetometer [SQUID; Quantum Design: (magnetic property measurement system) MPMS-XL] under an applied magnetic field of 10 Oe.

D. Crystal structure analysis

Room-temperature time-of-flight neutron powder-diffraction data were collected for both the AS ($s=1-4$) and the HPO ($s=1-3$) samples on the special environment powder diffractometer[21] at the Intense Pulsed Neutron Source. High-resolution backscattering data, from 0.5 to 4 Å d spacing were analyzed by the Rietveld analysis method using the general structure analysis system code (GSAS).[22,23] In the analysis, background, peak width, and extinction parameters were refined, together with the lattice parameters, atomic positions, and isotropic temperature factors.

III. RESULTS AND DISCUSSION

A. Phase formation

Normal-pressure sample synthesis in air yielded all the four (Cu,Mo)-12s2 phases in a single-phase form. Optimum formation temperatures for the four phases differ very slightly. However, we found that upon increasing the number of intervening (inserted) layers, significantly longer-heat treatment periods are required to complete the synthesis. The final single-phase composition is controlled by the starting Ce/Y cationic composition of the precursor. For all the four phases, Cu, Mo, and Sr contents were kept fixed whereas the total sum of Ce and Y and their optimal $Ce_{(s-1)}:Y_1$ ratio increased by increasing s. As such, the synthesis requirements are rather strict and all attempts to start with slightly different precursor compositions resulted in multiphase samples. Interestingly, with the optimal $Ce_{(s-1)}:Y_1$ ratio, the overall charge count of the (Ce,Y)-$[O_2$-(Ce,Y)$]_{s-1}$ block remains constant at 3+ independent of the layer number s (assuming nominal valence states of 4+ and 3+ for Ce and Y, respectively).

In order to get further insights into the phase-formation mechanism of the higher (Cu,Mo)-12s2 members, we monitored the phase evolution of the $s=4$ member by collecting several XRD patterns at intermediate synthesis steps. The sample was progressively annealed at 950–985 °C for a total of 48, 72, 96, 120, and 264 h. A small specimen was extracted from each intermediate product which was then subjected to HPO treatment followed by structural and superconducting characterization measurements. After 48 h annealing, see Fig. 1, the synthesized product mainly consists of the $s=3$ phase with significant traces of the $s=2$ and CeO_2 impurity phases still present. At this stage, no signs were detected for the $s=1$ member or the targeted $s=4$ phase.

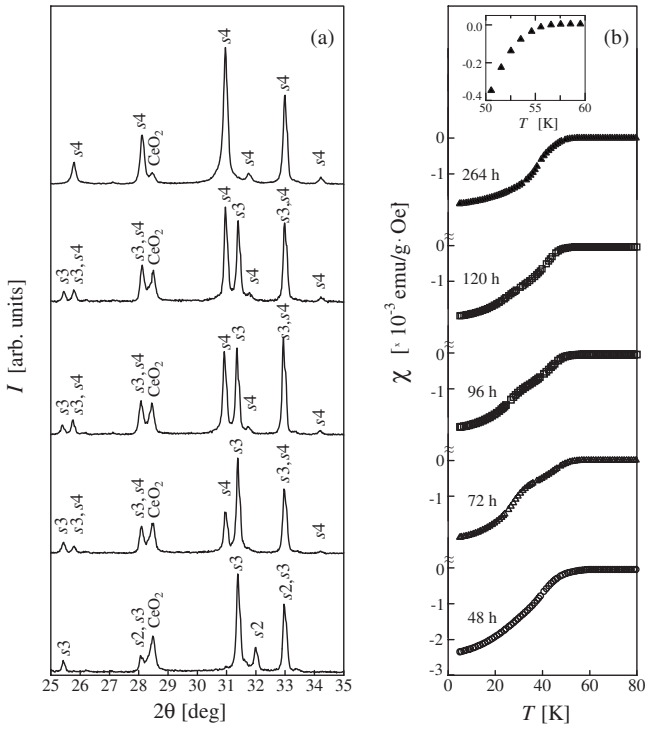

FIG. 1. (a) Evolution of the XRD patterns for the $(Cu_{0.75}Mo_{0.25})Sr_2(Ce_{0.75}Y_{0.25})_4Cu_2O_{13+\delta}$ sample synthesized from a nitrate precursor through several repeated heat treatments in air at 950–985 °C. (b) Magnetic-susceptibility data (for the corresponding HPO samples) with consecutive heat treatments. The given heat treatment duration indicates the total accumulated time used for the consecutive heat treatments.

However, as the figure also shows, the $s=4$ phase gradually evolves upon subsequent firing treatments with a concomitant decrease in the fractional amounts of CeO_2 and the lower s members. Magnetic-susceptibility curves for the mixed-phase intermediate products (after HPO annealing) exhibit broad or multiple transitions as displayed in Fig. 1. Only after the 264 h firing was complete, the product became essentially single-phase (Cu,Mo)-1242 with a sharp T_c of ~56 K (after HPO annealing). Our results demonstrate the slow phase formation of the higher s members of the (Cu,Mo)-12s2 series through the diffusive intercalation of individual CeO_2 layers (see structural results in subsequent paragraphs) into the (Ce,Y)-$[O_2$-$(Ce,Y)]_{s-1}$ fluorite-structured blocks of the lower s members starting from the $s=2$ phase rather than from the Ce-free $s=1$ phase.

B. Rietveld refinements and structural results

Refined crystal structure parameters for the $s=1-4$ phases are listed in Table I. In the refinements, structural models were constructed in which the designed layer repetition of SrO-$(Cu,Mo)O_{1\pm\delta}$-SrO-CuO_2-(Ce,Y)-$[O_2$-$(Ce,Y)]_{s-1}$-CuO_2 was confirmed. As shown in Figs. 2 and 3, our models successfully refined using the tetragonal symmetries of the $P4/mmm$ and $I4/mmm$ space groups for the $s=1$, 3 and $s=2$, 4 phases, respectively. No evidence was observed to justify the use of a lower structural symmetry as in the case, for example, of fully oxygenated $CuBa_2YCu_2O_{6+\delta}$ (Cu-1212).[24–26] We, therefore, conclude that the extra oxygen atoms in the HPO samples may at most form random chain fragments along the a or b direction; thus, resulting in an average tetragonal structure. Similar conclusions have previously been suggested for another closely related material, $Cu(Ba,La)_2(La,Ca)Cu_2O_{6+\delta}$.[27,28] In $Cu(Ba,La)_2(La,Ca)Cu_2O_{6+\delta}$ and underdoped $CuBa_2YCu_2O_{6+\delta}$ (i.e., before the formation of long-range ordered CuO_δ chains), the randomly distributed extra oxygen atoms in the CuO_δ layers are characterized by an asymmetric bonding with the surrounding cations and consequently in unusually large thermal factors indicative of disorder and significant local short-range displacements.

Initial refinements resulted in full occupancies for Cu2, O1, O2 ($s=1-4$), O3 ($s=2-4$), and O4 ($s=4$) within two or three standard deviations (see Table I for the atomic positions). The occupancies of these atoms were then kept fixed during the final refinements. No evidence for Mo substitution at the Cu2 site was observed (i.e., full Cu2 occupancies obtained with no unusual thermal factors or signs for displacements of the surrounding oxygen atoms). On the other hand, significantly large thermal factors were observed for Cu1 if Mo were not allowed to share the site. Strong structural correlations were observed when attempting to refine the individual Cu1 and Mo occupancies and the corresponding short-range displacements because of the complex local disorder associated with the Mo substitution and the lack of a significant neutron-scattering length contrast between Cu (7.718 fm) and Mo (6.715 fm). The formation of long-range Cu1/Mo order can be ruled out because of the absence of superstructure peaks that otherwise should have been observed.

Strong correlations were also observed when refining the site occupancies for Ce1/Y1 ($s=1-4$) and Ce2/Y2 ($s=3,4$). Interestingly, in every refinement model, the occupancy of Y2 always refined to values close to zero within 1–5 standard deviations, see Table I. We conclude that this site is mainly occupied by Ce in agreement with the observed intercalation mechanism (described above) of the Ce-O_2 double-layer block into the fluorite-structured blocks of the lower s members and the concomitant disappearance of the CeO_2 impurity phase.

On the other hand, the Ce1 and Y1 site occupancies always refined to values very close to the nominal ratios; thus, giving further support to the formation of "Ce-only" layers and Ce/Y mixed layers. Our refinement results suggest the random distribution of Ce and Y at the mixed Ce/Y site again with no evidence detected for any long-range cationic ordering.

As for the $(Cu,Mo)O_{1+\delta}$ layer, the proposed structures offer several possible sites for extra oxygen atoms at $(\frac{1}{2}\ \frac{1}{2}\ 0)$, $(\frac{1}{2}\ y\ 0)$, $(x\ x\ 0)$, $(x\ y\ 0)$, and $(\frac{1}{2}\ 0\ 0)$. Refinements of the different site occupancies led to the conclusion that the extra oxygen could partially occupy up to two of these sites, namely, O5 and O6 at the $(x\ y\ 0)$ and $(\frac{1}{2}\ y\ 0)$ sites, respectively, see Fig. 4. According to our model, the refined oxygen contents agree well with the anion stoichiometry as determined by titration ($s=1$) and x-ray absorption near-edge structure (XANES) measurements ($s=1-4$).[29]

TABLE I. Refined structural parameters for the AS ($s=1-4$) and HPO ($s=1-3$) members of the (Cu,Mo)-12s2 homologous series.

		$s=1$ (AS)	$s=1$ (HPO)	$s=2$ (AS)	$s=2$ (HPO)	$s=3$ (AS)	$s=3$ (HPO)	$s=4$ (AS)
T_c (K)		<4	87	<4	56	<4	54.5	<4 [a]
Sample weight (g)		0.25	0.12	6.79	0.23	6.7	0.48	0.63
χ^2		1.435	1.280	2.185	1.23	2.059	1.162	1.564
R_p (%)		5.68	9.11	4.94	5.63	5.91	3.07	3.83
R_{wp} (%)		7.72	12.41	6.49	7.56	8	4.14	5.28
Space group		$P4/mmm$	$P4/mmm$	$I4/mmm$	$I4/mmm$	$P4/mmm$	$P4/mmm$	$I4/mmm$
a (Å)		3.8280(4)	3.816(2)	3.83314(23)	3.8300(10)	3.83506(27)	3.8262(7)	3.8308(4)
c (Å)		11.5496(11)	11.471(8)	28.5614(18)	28.454(8)	16.9834(12)	16.9047(32)	39.344(4)
Vol. (Å^3)		169.24(5)	167.0(3)	419.65(8)	417.39(33)	249.79(5)	247.49(13)	577.36(18)
(Cu1,Mo)	0 0 0							
	U_{iso} (Å^2)	0.0301(9)	0.020(5)	0.0343(8)	0.0172(19)	0.0265(10)	0.0119(12)	0.0227(14)
Cu2	0 0 z							
	z	0.35680(16)	0.3503(10)	0.14505(5)	0.14350(20)	0.24250(13)	0.23967(24)	0.10463(11)
	U_{iso} (Å^2)	0.0056(4)	0.004(2)	0.00683(32)	0.0065(11)	0.0075(4)	0.0104(9)	0.0106(7)
Sr	$\frac{1}{2}$ $\frac{1}{2}$ z							
	z	0.19644(19)	0.186(1)	0.08146(6)	0.07704(24)	0.13581(15)	0.12826(32)	0.05883(11)
	U_{iso} (Å^2)	0.0194(6)	0.030(4)	0.0179(5)	0.0194(16)	0.0172(7)	0.0229(15)	0.0187(11)
(Ce,Y)1	$\frac{1}{2}$ $\frac{1}{2}$ z							
	z	0.5	0.5	0.20624(6)	0.20548(21)	0.34695(15)	0.34740(24)	0.14930(12)
	n(Y)	1.009(11)	1.00(6)	0.547(16)	0.56(5)	0.390(22)	0.43(4)	0.38(4)
	n(Ce)			0.453(16)	0.44(5)	0.610(22)	0.57(4)	0.62(4)
	U_{iso} (Å^2)	0.0069(7)	0.003(4)	0.0051(4)	0.005(1)	0.0015(6)	0.0005(10)	0.007(1)
(Ce,Y)2	0 0 z							
	z					0.5	0.5	0.21638(16)
	n(Y)					0.162(30)	0.02(6)	0.021(32)
	n(Ce)					0.838(30)	0.98(6)	0.979(32)
	U_{iso} (Å^2)					0.0072(11)	0.0045(22)	0.0012(11)
O1	0 0 z							
	z	0.15811(31)	0.163(1)	0.06458(9)	0.0663(3)	0.1082(2)	0.1106(4)	0.0460(2)
	U_{iso} (Å^2)	0.0274(9)	0.018(4)	0.0312(6)	0.022(2)	0.0292(9)	0.027(1)	0.024(1)
O2	$\frac{1}{2}$ 0 z							
	z	0.37461(14)	0.3703(9)	0.15109(4)	0.15086(13)	0.25387(11)	0.25268(19)	0.10959(7)
	U_{iso} (Å^2)	0.0085(4)	0.014(4)	0.01006(34)	0.0088(10)	0.0081(4)	0.0081(7)	0.0067(7)
O3	$\frac{1}{2}$ 0 z							
	z			0.25	0.25	0.42017(11)	0.41935(18)	0.18143(8)
	U_{iso} (Å^2)			0.0073(4)	0.0062(11)	0.0087(4)	0.0095(8)	0.0066(7)
O4	$\frac{1}{2}$ 0 z							
	z							0.25
	U_{iso} (Å^2)							0.0115(10)

TABLE I. (*Continued.*)

		$s=1$ (AS)	$s=1$ (HPO)	$s=2$ (AS)	$s=2$ (HPO)	$s=3$ (AS)	$s=3$ (HPO)	$s=4$ (AS)
O5	$x\ y\ 0$							
	x	0.582(8)		0.5940(30)	0.601(13)	0.605(4)	0.661(16)	0.604(4)
	y	0.260(12)		0.280(5)	0.252(19)	0.281(5)	0.280(16)	0.267(4)
	n	0.099(15)		0.070(6)	0.050(16)	0.085(7)	0.081(14)	0.121(9)
	U_{iso} (Å^2)	0.060(11)		0.011(5)	0.011(19)	0.019(6)	0.032(15)	0.018(6)
O6	$\frac{1}{2}\ y\ 0$							
	y	0.12(1)	0.16(2)	0.13(1)	0.09(1)	0.11(1)	0.10(1)	
	n	0.143(26)	0.39(1)	0.113(16)	0.252(29)	0.119(16)	0.267(23)	0
	U_{iso} (Å^2)	0.030(9)	0.04[b]	0.057(12)	0.026(9)	0.045(13)	0.036(8)	
Ox. cont.		7.36(16)	7.56(4)	9.01(8)	9.41(17)	11.16(9)	11.72(15)	12.97(7)

[a]T_c for the HPO superconducting $s=4$ sample is 55.5 K.
[b]Fixed.

C. Bond lengths and bond valence sums

With increasing the number s of the cation layers in the (Ce,Y)-$[O_2$-$(Ce,Y)]_{s-1}$ block, both the c axis and the interatomic distance $d_{(Cu\text{-}Cu)}$ (through this block) increase linearly. The a-axis parameter, on the other hand, remains nearly unchanged, Fig. 5. The HPO treatment results in slight lattice contractions in both the in-plane (0.1–0.3 %) and the out-of-plane (0.4–0.7 %) directions in agreement with the behavior of many other high-T_c superconductors, e.g., $CuBa_2YCu_2O_{6+\delta}$ (Ref. 30) (commonly referred to as YBCO) upon oxygenation.

Select interatomic bond lengths and angles are listed in Table II. The use of these bond length values in conjunction

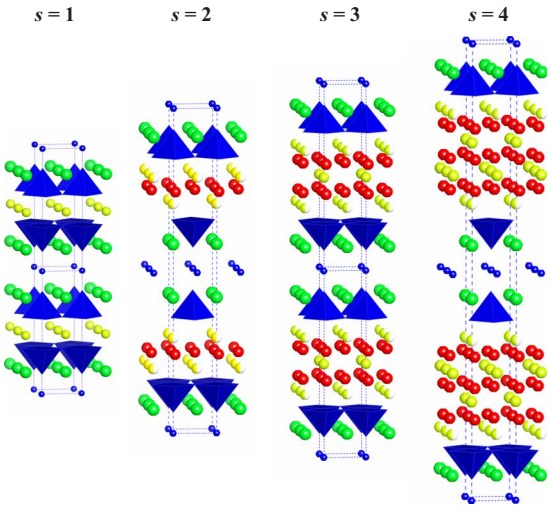

FIG. 2. (Color online) Crystal structures of (Cu,Mo)-12s2. Tetragonal $P4/mmm$ ($s=1,3$) and $I4/mmm$ ($s=2,4$). For simplicity, the O5 and O6 oxygen atoms have been omitted from the $(Cu_{0.75}Mo_{0.25})O_{1+\delta}$ planes. Labels: dark/blue pyramids ($Cu2O_5$), small/blue spheres (Cu1,Mo), medium dark/green spheres (Sr), light/solid yellow spheres (Y), dark/red spheres (O), and half-shaded/half-yellow half-white spheres (Y,Ce).

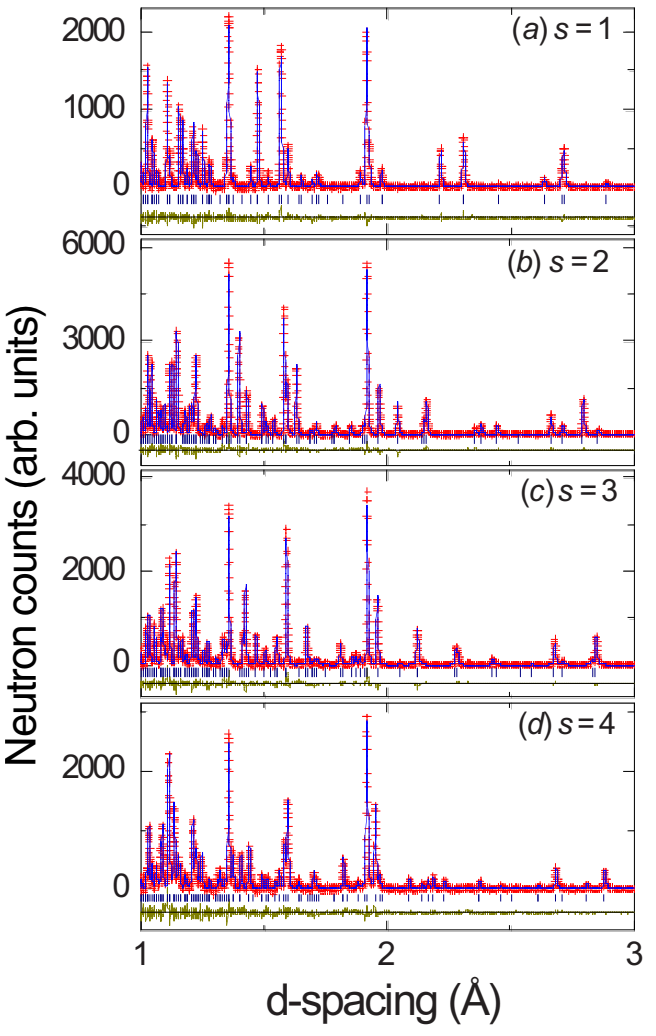

FIG. 3. (Color online) Best fit Rietveld refinements for (a) (Cu,Mo)-1212, (b) (Cu,Mo)-1222, (c) (Cu,Mo)-1232, and (d) (Cu,Mo)-1242.

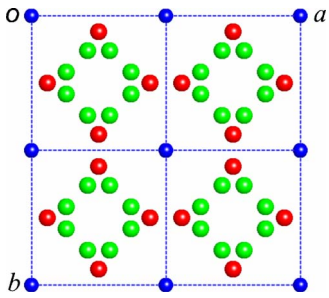

FIG. 4. (Color online) The $(Cu,Mo)O_{1+\delta}$ layer. Atomic positions for the extra oxygen atoms O5 (x y 0; green or light shade) and O6 ($\frac{1}{2}$ y 0; red or dark shade) are shown. The sites are only partially occupied. Blue spheres (corners) represent Cu/Mo.

with Brown and Altermatt's method and Zachariasen's bond valence sum equation, $v=\Sigma e^{(r_o-r_{ij})/B}$, where $B=0.37$, r_{ij}=the bond lengths between each cation and its first anionic neighbors, and r_o=empirical values determined from complex oxides, resulted in oxidation state values suggestive of Y^{3+}, Ce^{4+} (at both sites), and $Cu2^{\langle 2.21+\rangle}$ for the nonsuperconducting AS samples (Table II). The Cu2 oxidation state increases sensibly to 2.45+ and 2.32–2.34+ for the HPO $s=1$ and $s=2$, 3 samples, respectively (see Table II). For the superconducting $s=1$ sample, it is important to note the agreement between its high T_c (Table I) and its average Cu2 oxidation state and the previously reported XANES results.[29] It is also worth noting the difference in Cu2 oxidation state before and after high-pressure annealing [$\sim$0.24+ ($s=1$) and $\sim$0.1–0.12 ($s=2,3$)] again in agreement with the XANES results.[29] In this work, r_o values of 2.019, 2.116, 2.074, 1.655, and 1.735 determined from similarly complex oxide structures were used for Y^{3+}, Ce^{3+}, Ce^{4+}, Cu^{2+}, and Cu^{3+}, respectively.[31–37] The average oxidation state for Cu2 in the CuO_2 layers was calculated according to the method described in Ref. 27.

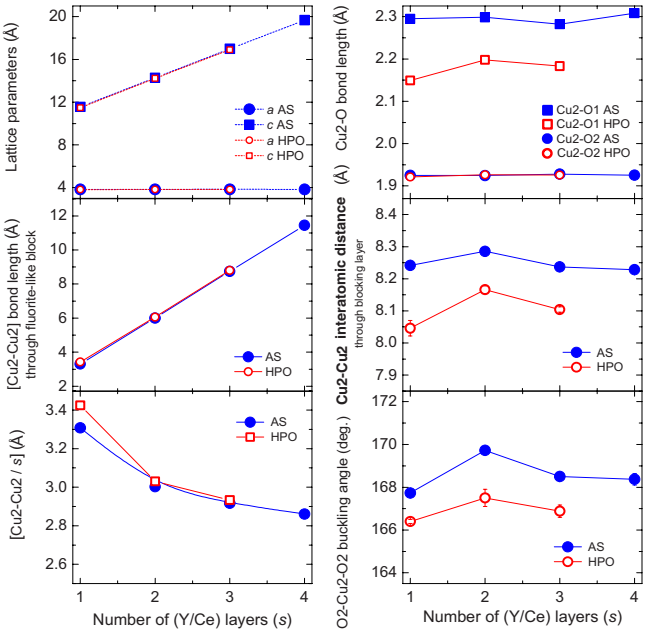

FIG. 5. (Color online) Lattice parameters, bond lengths, and angles as a function of layer number s. For the $s=2$ and 4 samples, the c axes are divided by a factor of 2.

As expected, the length of the Cu2-(Ce,Y)-$[O2-(Ce,Y)]_{s-1}$-Cu2 fluorite-structured block increases linearly from $\sim$3 to 12 Å upon increasing the layer number s but the average block thickness normalized to only one (Ce,Y) layer [i.e., $(Cu2-Cu2)/s$] decreases upon increasing s, Fig. 5. This result suggests that the increased thickness of the insulating fluorite block would weaken the electron tunneling between the CuO_2 layers (through the fluorite-type blocks); thus, reducing the three-dimensional character of the CuO_2 superconducting blocks. However, we would like to point out that in this homologous series, the reservoir block SrO-$(Cu,Mo)O_{1+\delta}$-SrO is more oxygenated than in similar cuprates as, for example, in $CuBa_2YCu_3O_7$ or more appropriately in $CuSr_2YCu_3O_7$. As we will see below in the HPO phases an appreciable fraction of the Cu cations are five or even six coordinated while they are only four coordinated in $CuBa_2YCu_3O_7$ or in the Sr counterpart.

We observe no significant effects before and after oxygenation on the various (Ce,Y)-O bond lengths and the Ce oxidation state remains unchanged. We thus conclude that no competition exists between Ce and Cu2 with respect to attracting the extra charges introduced by oxygen doping.

On the other hand, the out-of-plane O2-Cu2-O2 buckling angle becomes significantly larger for the superconducting samples in a counterintuitive disagreement with the common belief that maximum T_c's are achieved when perfectly flat CuO_2 planes are synthesized. Noting the similar results obtained with Cu-1212-type structures (at constant oxygen doping amounts),[28,38] we interpret this result as evidence for a direct competition between the electronic and nuclear structures (i.e., structural instabilities and electronic density of states) of the superconducting materials. Thus, higher T_c's should be possible, for similar oxygen contents, if flatter CuO_2 planes (less buckling) could be synthesized.

D. Structural correlations with superconductivity

In order to understand the structural details in terms of their effects on superconductivity, we propose in Fig. 6 a short-range ordered model for the $(Cu1,Mo)O_{1+\delta}$ layers (a) before and (c) after oxygenation [corresponding tilted views are displayed in (b) and (d), respectively]. The orthorhombic arrangement in these drawings and the absence of superstructure ordering peaks in the average tetragonal structure indicate that small domains extending to at most 100 unit cells or so ($\sim$400 Å) may exist along the a and b axes.

The significance of this model, albeit may not be unique, is that it describes well the structural results and the observed T_c behavior across the whole series. Starting with the $s=1$ AS sample, the refinement gives partial oxygen occupancies of 58% of O5 (x y 0) and 42% of O6 ($\frac{1}{2}$ y 0). All the Mo cations (one fourth of the total positions) are six coordinated while only a few of the Cu1 atoms have this type of coordination. The remaining Cu1 atoms are squarely coordinated just like they are in the structure of oxygenated CuBa2YCu2$O_{6+\delta}$.

The structure of HPO $s=1$ may be easier to understand. The O5 (x y 0) positions disappear in favor of the more

TABLE II. Select bond lengths and angles for the AS ($s=1-4$) and HPO ($s=1-3$) members of the (Cu,Mo)-12s2 homologous series. Oxidation states are calculated for Ce, Y, and Cu2.

Bond length	Multiplicity	$s=1$ (AS)	$s=1$ (HPO)	$s=2$ (AS)	$s=2$ (HPO)	$s=3$ (AS)	$s=3$ (HPO)	$s=4$ (AS)
(Cu1,Mo)-O1	×2	1.826(4)	1.874(18)	1.8444(25)	1.885(7)	1.8369(35)	1.869(6)	1.809(6)
(Cu1,Mo)-O5	[a]	1.885(18)		1.890(11)	1.81(4)	1.861(14)	1.681(28)	1.830(16)
(Cu1,Mo)-O5	[a]	2.44(4)		2.516(15)	2.50(6)	2.557(19)		2.528(16)
(Cu1,Mo)-O6	[a]	1.968(8)	2.002(10)	1.980(10)	1.946(5)	1.962(8)	1.953(4)	
Cu2-O1	×1	2.295(4)	2.149(20)	2.2984(32)	2.198(9)	2.282(4)	2.183(7)	2.308(7)
Cu2-O2	×4	1.9250(3)	1.9215(23)	1.92432(22)	1.9264(9)	1.92723(31)	1.9257(6)	1.9253(5)
Sr-O1	×4	2.7428(8)	2.7113(30)	2.7530(5)	2.7255(14)	2.7522(7)	2.7221(11)	2.7556(12)
Sr-O2	×4	2.8104(19)	2.846(14)	2.7619(15)	2.842(6)	2.7743(22)	2.843(5)	2.767(4)
Sr-O5		2.468(15)		2.501(6)	2.420(27)	2.487(7)	2.406(13)	2.513(8)
Sr-O6		2.696(19)	2.504(20)	2.725(20)	2.696(18)	2.754(21)	2.648(14)	
(Ce,Y)1-O2	×4	2.400(1)	2.417(7)	2.4809(14)	2.466(4)	2.4852(20)	2.4947(34)	2.472(4)
(Ce,Y)1-O3	×4	2.400(1)	2.417(7)	2.2880(9)	2.2961(33)	2.2854(18)	2.2671(29)	2.2950(33)
	×8 ($s=3$)							
(Ce,Y)2-O3	×4 ($s=4$)					2.3472(27)	2.3492(18)	2.358(5)
(Ce,Y)2-O4	×4							2.328(4)
O2-Cu2-O2		167.73(15)	166.4(10)	169.72(12)	167.5(4)	168.50(16)	166.88(29)	168.37(27)
BVS(Cu2)		2.21	2.45	2.22	2.31	2.22	2.34	2.20
v(Cu2) from XANES[c]			2.53		2.28		2.26	2.27[b]
v(Y1)		2.87	2.73	3.08	3.09	3.10	3.15	3.07
v(Y2)						3.29	3.28	
v(Ce1)				3.57	3.58	3.60	3.66	3.57
v(Ce2)						3.82	3.80	3.87

[a]Site multiplicity × oxygen fractional occupancies.
[b]For the $s=4$ HPO sample.
[c]Reference 29.

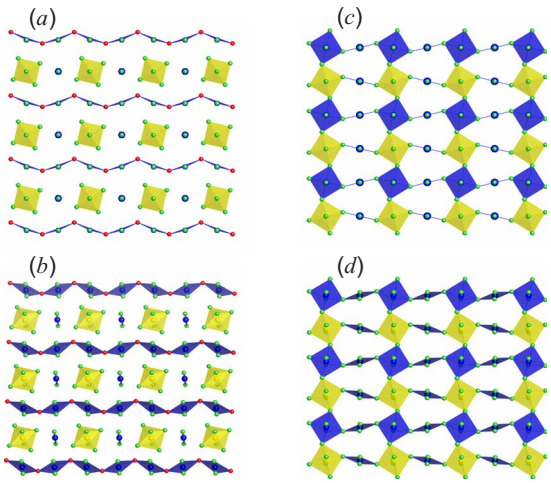

FIG. 6. (Color online) View along the [001] direction for the short-range ordered (Cu1,Mo)$O_{1+\delta}$ models (a) before and (c) after oxygenation. Tilted views are displayed in (b) and (d) to show the various Cu coordinations in the AS and HPO samples.

symmetrical O6 ($\frac{1}{2}$ y 0) positions. The local structure should be orthorhombic but the domain model applies in this case as well. In this model, the O6 occupancy factor corresponds to 0.375 which is in very good agreement with the refined value of 0.39(1). All Mo are octahedrally coordinated whereas the number of six coordinated Cu1 increases to 1/3 which corresponds to $\delta=0.5$. The remaining 2/3 Cu1 atoms are squarely coordinated.

The occupancy of the basal plane for the $s=2$ AS sample is exactly the same as that of the $s=1$ AS sample. The occupancy of the (x y 0) positions is 55% which is within one or two standard deviations from the value for the $s=1$ AS sample. In the case of $s=2$, high-pressure oxygenation increases the occupancy of the more symmetrical O6 site but the occupancy of O5 does not drop to 0 as in the case of $s=1$. The relative O5/O6 occupancies change from 55%/45% to 36%/64% before and after oxygenation, respectively. Some oxygen ordering takes place by oxygenation but not as well as for the $s=1$ sample. The case of the $s=3$ sample is similar with the relative O5/O6 occupancies changing from 59%/41% to 38%/62% after oxygenation. It is interesting to note that in the $s=4$ AS sample, all the oxygen atoms are in the O5 (x y 0) positions. We tentatively explain this order-

ing as due to the long time required for the synthesis of this material (a couple of weeks) which may give enough time for the oxygen atoms to settle/order around the Mo cations. Since the $s=4$ HPO sample is also superconducting at 55.5 K, one could anticipate that oxygen ordering would take place at the O6 site as well.

Our structural results seem to offer an explanation as why the T_c of 87 K for the Mo-substituted $s=1$ sample is significantly higher than the T_c's of the unsubstituted parent $CuSr_2YCu_2O_{6+\delta}$ material (~60 K or less),[39–42] and why the higher s members of the series exhibit lower and more importantly constant T_c's of ~55 K. The higher oxidation of the $(Cu_{0.75}Mo_{0.25})O_{1+\delta}$ layer accompanied by oxygen ordering is responsible for the higher T_c of $(Cu_{0.75}Mo_{0.25})Sr_2YCu_2O_{7+\delta}$. The insertion of the insulating (Ce,Y)-$[O_2$-$(Ce,Y)]_{s-1}$ blocks must drastically change the scenario that the three dimensionality of superconductivity occurs via Josephson coupling through these insulating blocks. By carefully examining the four structures presented in Fig. 2, one can see an immediate drop in dimensionality as s increases from 1 to 2 or higher. It is quite clear that the structures for the $s=2-4$ members all present single superconducting blocks; i.e., CuO_2-SrO-$(Cu,Mo)O_{1+\delta}$-SrO-CuO_2, separated by insulating layers of various thicknesses; thus, explaining the constant T_c values for these members. The incomplete oxygen ordering in the $s=2$ and 3 HPO samples results in lessening the effectiveness of the charge-transfer mechanism to the superconducting CuO_2 planes and consequently in lowering T_c's.

As described above, our samples are either optimally doped or very slightly underdoped. Thus, for our HPO samples, oxygen content is not the parameter responsible for the different maximal T_c's. However, as previously demonstrated by Liu *et al.*[43] and Han *et al.*,[44] oxygen ordering outside the CuO_2 planes produces strong effects on superconductivity. Liu *et al.*'s low-temperature nitrogen annealing results obtained with Sr_2CuO_{3+d} materials show significant T_c enhancements from 75 to 89 K and 95 K that correlate with different modulated superstructures associated with oxygen-vacancy ordering at the apical oxygen sites. According to Liu *et al.*, local-density approximation band calculations show that ordering of the apical oxygen atoms would significantly affect the second-nearest hopping integral t' between two neighboring Cu-Cu atoms in the CuO_2 planes. Furthermore, they suggest that oxygen ordering correlates with minimized cationic disorder in the CuO_2 planes and within the SrO layers and results in enhanced T_c.

With this in mind, we similarly speculate that oxygen ordering in the $(Cu,Mo)O_{1+\delta}$-SrO-$(Cu,Mo)O_{1+\delta}$ charge-reservoir block significantly minimizes the cationic disorder that would otherwise occur at the (Cu,Mo) and Sr sites. Consequently, disorder at the apical oxygen site would also be minimized to result in enhanced charge transfer between the reservoir block and the CuO_2 planes. More work is needed in which the effects of oxygen ordering on T_c are fully investigated in samples produced to exhibit various degrees of oxygen order/disorder.

Finally, we note the familiar effects of oxygenation on the thickness of the Cu2-Cu2 blocking layer and on the apical Cu2-O1 bond length which exhibits a large contraction from ~2.3 Å (AS) to ~2.15 Å for the $s=1$ superconducting sample, Fig. 5. A relatively smaller contraction (2.3 Å to ~2.20 Å) is observed for the $s=2$, 3 members. On the other hand, the equatorial Cu2-O2 bond lengths remain unchanged before and after oxygenation. These results clearly indicate the important role played by the apical oxygen in facilitating the charge transfer between the $(Cu,Mo)O_{1+\delta}$ and CuO_2 layers.

IV. CONCLUSIONS

We have investigated the synthesis and structural properties of the (Cu,Mo)-12s2 homologous series of cuprate high-T_c superconductors. In this series, an insulating spacing or a blocking layer of constant total charge of +3, inserted between two adjacent superconductive CuO_2 planes, can be gradually thickened from ~3 Å for the single-cation Y layer in (Cu,Mo)-1212 to ~12 Å for the quadruple-fluorite-layered block in (Cu,Mo)-1242. For the $s=2-4$ samples, the value of T_c is not significantly affected by the extended blocking layer but rather on the constant hole-doping level in the CuO_2 planes as evidenced by neutron powder diffraction and previous XANES results. Analysis of the structures of (Cu,Mo)-12s2 reveals the presence of two independent crystallographic sites in the basal $(Cu_{0.75}Mo_{0.25})O_{1+\delta}$ layer that can accommodate the extra oxygen atoms introduced by high-pressure oxygen annealing. Significant oxygen redistribution appears to take place in the HPO annealed samples with complete short-range oxygen ordering taking place in the basal layer of the $s=1$ sample. On the other hand, only partial (incomplete) oxygen ordering takes place in the higher $s=2$ and 3 HPO samples, which seems to explain the reduced effectiveness in charge transfer to the CuO_2 superconducting layers and consequently in lowering their T_c's. The structural and unusual superconducting behavior of this homologous series clearly demonstrate the power of layer-by-layer engineering in achieving unique on-demand designs of high-T_c superconductors and related multilayered materials.

ACKNOWLEDGMENTS

This work was partly supported by Tekes under Grant No. 1726/31/07 and the Academy of Finland under Grants No. 116254 and No. 126528. I.G. acknowledges (Grant No. ID 043145) the Ministry of Education, Culture, Sports, Science and Technology of Japan. At Argonne, the work was supported by the U.S. Department of Energy, Office of Science, under Contract No. DE-AC02-06CH11357.

*Corresponding author; chmaissem@niu.edu

[1] For a review, see, M. Karppinen and H. Yamauchi, Mater. Sci. Eng. R. **26**, 51 (1999).

[2] C. Michel, M. Hervieu, M. M. Borel, A. Grandin, F. Dreslandes, J. Provost, and B. Raveau, Z. Phys. B: Condens. Matter **68**, 421 (1987).

[3] H. Maeda, Y. Tanaka, M. Fukutomi, and T. Asano, Jpn. J. Appl. Phys., Part 2 **27**, L209 (1988).

[4] Z. Z. Sheng and A. M. Hermann, Nature (London) **332**, 55 (1988); **332**, 138 (1988).

[5] C. C. Torardi, M. A. Subramanian, J. C. Calabrese, J. Gopalakrishnan, K. J. Morrissey, T. R. Askew, R. B. Flippen, U. Chowdry, and A. W. Sleight, Science **240**, 631 (1988).

[6] S. S. P. Parkin, V. Y. Lee, A. I. Nazzal, R. Savoy, R. Beyers, and S. J. La Placa, Phys. Rev. Lett. **61**, 750 (1988).

[7] S. Matsuda, S. Takeuchi, A. Soeta, T. Suzuki, K. Aihara, and T. Kamo, Jpn. J. Appl. Phys., Part 1 **27**, 2062 (1988).

[8] S. N. Putilin, E. V. Antipov, O. Chmaissem, and M. Marezio, Nature (London) **362**, 226 (1993).

[9] A. Schilling, M. Cantoni, J. D. Guo, and H. R. Ott, Nature (London) **363**, 56 (1993).

[10] M. Marezio, E. V. Antipov, J. J. Capponi, C. Chaillout, S. Loureiro, S. N. Putilin, A. Santoro, and J. L. Tholence, Physica B **197**, 570 (1994).

[11] A. Tokiwa, T. Oku, M. Nagoshi, and Y. Syono, Physica C **181**, 311 (1991).

[12] S. Ikegawa and Y. Motoi, Appl. Phys. Lett. **68**, 2430 (1996).

[13] T. Wada, A. Nara, A. Ichinose, H. Yamauchi, and S. Tanaka, Physica C **192**, 181 (1992).

[14] M. Karppinen, V. P. S. Awana, Y. Morita, and H. Yamauchi, Physica C **392-396**, 82 (2003); H. Fjellvåg, Y. Morita, T. Nagai, J. M. Lee, J. M. Chen, R. S. Liu, B. C. Hauback, V. P. S. Awana, Y. Matsui, H. Yamauchi, and M. Karppinen, J. Solid State Chem. **179**, 632 (2006).

[15] I. Felner, U. Asaf, Y. Levi, and O. Millo, Phys. Rev. B **55**, R3374 (1997).

[16] C. Bernhard, J. L. Tallon, Ch. Niedermayer, Th. Blasius, A. Golnik, E. Brücher, R. K. Kremer, D. R. Noakes, C. E. Stronach, and E. J. Ansaldo, Phys. Rev. B **59**, 14099 (1999).

[17] H. Sasakura, Y. Akagi, S. Noguchi, S. Tsukui, T. Oka, and M. Adachi, J. Supercond. **16**, 961 (2003).

[18] E. Kandyel, A. Yamamoto, and S. Tajima, Physica C **341-348**, 429 (2000).

[19] T. Watanabe, M. Karppinen, T. Motohashi, T. Nagai, Y. Matsui, and H. Yamauchi, Phys. Rev. B **70**, 174514 (2004).

[20] Y. Morita, T. Nagai, Y. Matsui, H. Yamauchi, and M. Karppinen, Phys. Rev. B **70**, 174515 (2004); M. Karppinen, Y. Morita, T. Kobayashi, I. Grigoraviciute, J. M. Chen, R. S. Liu, and H. Yamauchi, J. Solid State Chem. **178**, 3464 (2005); I. Grigoraviciute, H. Yamauchi, and M. Karppinen, J. Am. Chem. Soc. **129**, 2593 (2007).

[21] J. D. Jorgensen, J. J. Faber, J. M. Carpenter, R. K. Crawford, J. R. Haumann, R. L. Hitterman, R. Kleb, G. E. Ostrowski, F. J. Rotella, and T. G. Worlton, J. Appl. Crystallogr. **22**, 321 (1989).

[22] A. C. Larson and R. B. von Dreele, Los Alamos National Laboratory Report No. LAUR 86–748, 2000 (unpublished).

[23] B. H. Toby, J. Appl. Crystallogr. **34**, 210 (2001).

[24] W. I. F. David, W. T. A. Harrison, J. M. F. Gunn, O. Moze, A. K. Soper, P. Day, J. D. Jorgensen, D. G. Hinks, M. A. Beno, L. Soderholm, D. W. Capone, I. K. Schuller, C. U. Segre, K. Zhang, and J. D. Grace, Nature (London) **327**, 310 (1987).

[25] E. A. Hewat, M. Dupuy, A. Bourret, J. J. Capponi, and M. Marezio, Nature (London) **327**, 400 (1987).

[26] J. D. Jorgensen, M. A. Beno, D. G. Hinks, L. Soderholm, K. J. Volin, R. L. Hitterman, J. D. Grace, I. K. Schuller, C. U. Segre, K. Zhang, and M. S. Kleefisch, Phys. Rev. B **36**, 3608 (1987).

[27] O. Chmaissem, Y. Eckstein, and C. G. Kuper, Phys. Rev. B **63**, 174510 (2001).

[28] O. Chmaissem, J. D. Jorgensen, S. Short, A. Knizhnik, Y. Eckstein, and H. Shaked, Nature (London) **397**, 45 (1999).

[29] I. Grigoraviciute, M. Karppinen, T. S. Chang, J. M. Chen, R. S. Liu, O. Chmaissem, and H. Yamauchi, J. Am. Chem. Soc. **132**, 838 (2010).

[30] J. D. Jorgensen, B. W. Veal, A. P. Paulikas, L. J. Nowicki, G. W. Crabtree, H. Claus, and W. K. Kwok, Phys. Rev. B **41**, 1863 (1990).

[31] I. D. Brown and D. Altermatt, Acta Crystallogr., Sect. B: Struct. Sci. **41**, 244 (1985).

[32] A. Trzesowska, R. Kruszynski, and T. J. Bartczak, Acta Crystallogr., Sect. B: Struct. Sci. **60**, 174 (2004).

[33] A. Trzesowska, R. Kruszynski, and T. J. Bartczak, Acta Crystallogr., Sect. B: Struct. Sci. **62**, 745 (2006).

[34] G. P. Shields, P. R. Raithby, F. H. Allen, and W. D. S. Motherwell, Acta Crystallogr., Sect. B: Struct. Sci. **56**, 455 (2000).

[35] S. Mahapatra, J. A. Halfen, E. C. Wilkinson, G. F. Pan, X. D. Wang, V. G. Young, C. J. Cramer, L. Que, and W. B. Tolman, J. Am. Chem. Soc. **118**, 11555 (1996).

[36] W. H. Zachariasen, Acta Crystallogr. **7**, 795 (1954).

[37] W. H. Zachariasen, Acta Crystallogr. **16**, 385 (1963).

[38] J. D. Jorgensen, O. Chmaissem, D. G. Hinks, A. Knizhnik, Y. Eckstein, H. Shaked, J. L. Wagner, B. Dabrowski, S. Short, J. F. Mitchell, and J. P. Hodges, *High-Temperature Superconductors and Novel Inorganic Materials* (Kluwer Academic, The Netherlands, 1999), Vol. 62, p. 109.

[39] E. Gilioli, P. G. Radaelli, A. Gauzzi, F. Licci, and M. Marezio, Physica C **341-348**, 605 (2000).

[40] A. Prodi, A. Gauzzi, E. Gilioli, F. Licci, M. Marezio, F. Bolzoni, G. Allodi, R. De Renzi, F. Bernardini, S. Massidda, G. Profeta, A. Continenza, and P. G. Radaelli, Int. J. Mod. Phys. B **17**, 873 (2003).

[41] O. I. Lebedev, G. Van Tendeloo, F. Licci, E. Gilioli, A. Gauzzi, A. Prodi, and M. Marezio, Phys. Rev. B **66**, 132510 (2002).

[42] Y. Cao, T. L. Hudson, Y. S. Wang, S. H. Xu, Y. Y. Xue, and C. W. Chu, Phys. Rev. B **58**, 11201 (1998).

[43] Q. Q. Liu, H. Yang, Y. Yu, L. X. Yang, R. C. Yu, F. Y. Li, C. Q. Jin, and S. Uchida, Physica C **463-465**, 100 (2007).

[44] P. D. Han, L. Chang, and D. A. Payne, Physica C **228**, 129 (1994).